River Flow 2010 - Dittrich, Koll, Aberle & Geisenhainer (eds) - © 2010 Bundesanstalt für Wasserbau ISBN 978-3-939230-00-7

Three Dimensional Numerical Modeling of Flow around Bridge Piers Using LES and RANS

Y. Aghaee & H. Hakimzadeh
Faculty of Civil Engineering, Sahand University of Technology, Tabriz, Iran

ABSTRACT: Details are given of a three-dimensional numerical model study to simulate the turbulent flow around a vertical circular pier. The developed model is based on the solution of fully three-dimensional hydrodynamic equations. These equations can be achieved with two different methods, including:-1) Reynolds Averaged Navier-Stokes equations (RANS) and 2) Space Averaged Navier-Stokes equations. For the turbulence models the two-equation standard k-ε model of RANS type and the Smagorinsky model of large eddy simulation (LES) type have been deployed for each set of the hydrodynamic equations. The governing equations were discretized using the structured mesh of cell-centered collocated finite volume method, with the convection and diffusion terms being discretized using the third order upwind and second order central schemes, respectively. Also in order to discretize the temporal terms a five-stage forth-order accurate Runge–Kutta scheme has been used. The pressure-velocity coupling has been achieved using the artificial compressibility method. Based on extensive numerical tests, the capability and the performance of the LES and RANS models have been validated against experimental data. Then, the numerical model results of the velocity, pressure and bed shear stress fields were compared with the available two sets of experimental data. The numerical model results showed that the length and intensity of the wake and also the horseshoe vortices are mainly affected with the turbulence models used.

Keywords: 3D numerical model, Finite volume, Artificial compressibility method, Circular pier, LES, RANS

1 INTRODUCTION

Cylindrical bridge piers are among the most commonly used structures in coastal, offshore and river engineering. The scouring process and forces on these hydraulic structures due to river current are very important subjects in river engineering and must be considered carefully. The formation of local scour hole around bridge piers is closely related to the fluid flow characteristics near the bed and around the pier. The characteristics of flow pattern around the vertical circular piers are obviously fully three dimensional and complicated. The scour process around the bridge piers is a dynamic and unsteady process and is still a prominent phenomenon that needs to be considered by many researchers. There are a large number of investigations for the flow field around the circular piers both numerically and experimentally. Experimental observation has demonstrated that the horseshoe vortices have the basic role of the scour around the bridge piers (Dargahi, 1990). Dargahi also showed the formation of the horseshoe vortex around the circular pier and its frequent manner (Dargahi, 1989).

The main purpose of a numerical simulation of flow around the bluff bodies such as circular pier in the rivers is to estimate the bed shear stress and consequently the scour hole. These features are closely related to the turbulence models used for simulation. Direct numerical simulation (DNS) method is the most accurate solution among the others. However, its performance has been restricted to the low Reynolds number (Re) and needs to a high performance computer. Yuhi et al. (2000) studied the effects of bottom topographies on the formation of the horseshoe vortex with DNS numerical modeling. Also, Gushchin et al. (2002) investigated transitional regimes of separated fluid flows around a circular cylinder up to the Reynolds of 400 using DNS method. Wissink & Rodi (2008) performed a series of direct numer-

ical simulations of incompressible flow around a circular cylinder at Re of 3300 to 3900 and with the maximum grid number of about 5×10^8. Many of researchers have also studied the flow fields around circular piers with various turbulence models of RANS types, including: Majumdar & Rodi (1989), Olsen & Melaeen (1993), Nagata et al. (2000), Salaheldin et al. (2004), Roulund et al. (2005). Nowadays due to the relatively high performance of the computers, numerical simulation of the flow fields with large eddies is more practical. The intermediate approach between (DNS) and (RANS) is the well-known large-eddy simulation (LES) method. In this research study, the three-dimensional time dependent Navier-Stokes equations are numerically solved. Since at higher Reynolds numbers, the small scale turbulent motions can not be resolved in such calculations, it is filtered out and only motions larger than the filter width are resolved (Rodi, 1997). Various turbulent models may also produce different results for flow fields and eventually different scour estimations.

In this paper two different turbulence models have been adopted for simulating the flow field around the mounted circular pier on a rigid bed. The models are based on the solution of two different approaches: 1)Reynolds Averaged Navier-Stokes equations (RANS) using the standard k-e model and 2)Space averaged Navier-Stokes equations using large eddy simulation (LES) with the standard Smagorinsky (1963) sub-grid-scale model. The results of two different models have been compared with each other. They are also validated with two sets of experimental data, namely, 1) Roulund et al. (2005) and 2) Dargahi (1989).

2 NUMERICAL MODEL

2.1 *LES and RANS*

The three-dimensional Navier-Stokes and continuity equations can be written for two different LES and RANS approach similarly as follows:

$$\frac{\partial \overline{u_i}}{\partial x_i}=0 \tag{1}$$

$$\frac{\partial \overline{u_i}}{\partial t}+\frac{\partial \overline{u_i}\,\overline{u_j}}{\partial x_j}=-\frac{1}{\rho}\frac{\partial \overline{P}}{\partial x_i}+\nu\left(\frac{\partial^2 \overline{u_i}}{\partial x^2{}_j}\right)+\left(\frac{\partial \tau_{ij}}{\partial x_j}\right) \tag{2}$$

where x_i=*1, 2, 3* denotes the stream-wise, span-wise and vertical directions, respectively, $\overline{u_i}$= time averaged or filtered velocity components in the mentioned directions, $\overline{P}$ = time averaged or filtered pressure, ρ = density, ν = kinematic viscosity of the fluid, and τ_{ij} = Reynolds shear stresses or sub-grid shear stresses.

The effect of unresolved scale motion in LES is appeared on the sub-grid scale shear stress tensor that should be modeled. The common method for modeling of the sub-grid scale is similar to eddy-viscosity concept method, given as:

$$\tau_{ij}-\frac{1}{3}\tau_{kk}\delta_{ij}=\nu_t\left(\frac{\partial \overline{u_i}}{\partial x_j}+\frac{\partial \overline{u_j}}{\partial x_i}\right)=2\nu_t\overline{S_{ij}} \tag{3}$$

where ν_t = eddy viscosity and may be found as:

$$\nu_t=l_S{}^2\left|\overline{S}\right| \tag{4}$$

$$\left|\overline{S}\right|=\left(2\overline{S_{ij}}\,\overline{S_{ij}}\right)^{1/2} \tag{5}$$

where l_s = mixing length for sub-grid scales. Taking into account the reduction of the sub-grid length near solid walls, the length scale is usually multiplied by a Van Driest damping function, as (Breuer 1998):

$$l_S=C_S\Delta^{1/3}\left[1-\exp\left(-\frac{z^+}{25}\right)^3\right]^{0.5} \tag{6}$$

where C_s = the Smagorinsky parameter chosen equal to 0.1 for this investigation. Δ = volume of the mesh, $\overline{S_{ij}}$ = strain rate; $z^+=\frac{zu_*}{\nu}$; u_* = friction velocity base on the wall shear stress; z = distance of the first grid center from wall.

The most popular method for RANS modeling is the standard *k*-ε model. In this model the turbulence field is introduced in terms of the turbulent kinetic energy (*k*) and its rate of dissipation (ε). The equations of the temporal changes of *k* and ε can then be written as follows:

$$\frac{\partial k}{\partial t}+\frac{\partial \overline{u_i}k}{\partial x_j}=\frac{\partial}{\partial x_j}\left(\frac{\nu_t}{\sigma_k}\frac{\partial k}{\partial x_j}\right)+P-\varepsilon \tag{7}$$

$$\frac{\partial \varepsilon}{\partial t}+\frac{\partial \overline{u_i}\varepsilon}{\partial x_j}=\frac{\partial}{\partial x_j}\left(\frac{\nu_t}{\sigma_\varepsilon}\frac{\partial \varepsilon}{\partial x_j}\right)+C_{1\varepsilon}\frac{\varepsilon}{k}P-C_{2\varepsilon}\frac{\varepsilon^2}{k} \tag{8}$$

$$P=\nu_t\left(\frac{\partial \overline{u_i}}{\partial x_j}+\frac{\partial \overline{u_j}}{\partial x_i}\right)\frac{\partial \overline{u_i}}{\partial x_j} \tag{9}$$

$$\nu_t=C_\mu\frac{k^2}{\varepsilon} \tag{10}$$

In the above equations there are five constants that should be prescribed as: $C_\mu=0.09$, $C_{1\varepsilon}=1.44$, $C_{2\varepsilon}=1.92$, $\sigma_k=1.0$ and $\sigma_\varepsilon=1.3$.

Boussinesq proposed the eddy viscosity concept to determine the Reynolds stresses as:

$$\tau_{ij} = (-\overline{u_i' u_j'}) = \nu_t \left(\frac{\partial \overline{u_i}}{\partial x_j} + \frac{\partial \overline{u_j}}{\partial x_i} \right) - \frac{2}{3} k \delta_{ij} \quad (11)$$

where δ_{ij} = the kroneker delta.

2.2 *Method of solution*

The Artificial Compressibility method (AC), proposed by Chorin (1967), has been adopted to solve the three-dimensional Navier-stokes equations. In this method, the artificial compressibility parameter β (which is related to an artificial speed of the sound) enables the set of equations to converge to a solution satisfying the incompressibility condition. Continuity equation (1) in AC method is then modified by the first term, as given:

$$\frac{1}{\rho \beta^2} \frac{\partial P}{\partial t} + \frac{\partial \overline{u_i}}{\partial x_i} = 0 \quad (12)$$

For the unsteady simulation of Navier-Stokes equations, solution is achieved by using dual time stepping or single time stepping with larger artificial compressibility parameter (Louda et al. 2008). The faster convergence for a small time step of the numerical model is obtained by choosing larger β s (Kim & Menon, 1999). In this investigation the single time method and the constant β (which is higher than the order of the maximum flow velocity) are selected.

Also, the finite-volume method (FVM) has been used on the structured grids to calculate the 3D unsteady incompressible Navier–Stokes equations. Temporal discretization has been done with an explicit five-stage forth-order accurate Runge–Kutta scheme. For the artificial compressibility method in order to get the unsteady solution with a single time step, the accuracy of more than the first order is vital. Explicit time marching works well for LES with the small time steps being necessary to resolve turbulence motion in time (Breuer 1998). A collocated finite-volume discretization was used with the third order upwind (Leonard 1975) and second order central schemes being deployed for the convection and diffusion terms, respectively. Also, in order to rectify the problem of the unphysical pressure oscillation occurred in the non-staggered grids, the momentum interpolation method (MIM) proposed by (Rhie & Chow 1983) has been used.

2.3 *Boundary condition*

For the governing equations the following boundary conditions have been imposed. A uniform velocity profile ($u = u_0$, $v = w = 0$) and Neumann boundary condition for velocity ($\partial \overline{u_i} / \partial n = 0$) are used at the inlet and outlet boundaries, respectively, where u_0 = the inlet velocity and n = the normal direction to the boundaries. For the solid walls (pier surface) the no-slip boundary condition was used; for free surface the rigid lid with symmetry condition and free slip condition are imposed. For the pressure in all boundaries the Neumann condition is imposed except for the outlet in which the following relation is used (Gersho 1991):

$$P_{outlet} = 2\mu \left(\frac{\partial u_n}{\partial n} \right) \quad (13)$$

where μ = the dynamic viscosity of the fluid.

Moreover, in using the rigid lid concept the following point has to be considered with more care. The difference in the surface elevation between the front and side edges of the cylinder may, to a first approximation, be written as $\Delta h / h = Fr^2$ for small Froude numbers. Using this relation, it can be seen that $\Delta h / h$ < O(0.02), a 'head' difference which is small enough not to cause any significant flow in the radial direction (practically no Froude-number effect) when Fr < O(0.2). At this stage, it may be noted that the Froude number in the most practical cases (except mountainous streams) is very small, certainly smaller than O(0.2), and therefore the present numerical model (without the free surface 'facility') can be used with no serious implications (Roulund et al. 2005). The advantage of the rigid lid assumption is that it does not require a vast amount of CPU time as for the free surface model (Tseng et al. 2000).

The following expression was used for the bed shear stress (Hakimzadeh & Falconer, 2007):

$$\tau_0 = \rho u (u^2 + v^2)^{0.5} \left[2.5 \ln \left(\frac{30d}{k_S} \right) \right]^{-2} \quad (14)$$

where d = the thickness of the bed layer and k_s = Nickorades roughness of the bed material. Also, for the RANS modeling the wall function was used for simulation of the flow near the bed and cylinder in which, the first grid near the wall must be located at the outside of the viscous sub-layer in the range of $30 < z^+ < 100$. Near the bed the solution is related to the wall function and local equilibrium of turbulence in which production equals to the dissipation of the kinetic energy (Li & Yu 1996):

$$k_{bed} = \frac{{u_*}^2}{C_\mu^{0.5}} \quad (15)$$

$$\varepsilon_{bed} = \frac{{u_*}^3}{0.42d} \quad (16)$$

The Neumann condition has been used when the wall was rough and transitional where $(\partial k/\partial n = 0)$ was satisfied. At the outlet and free surface the Neumann condition was imposed, for the inlet, however, the following expressions were used:

$$k_{in} = 0.0005{u_0}^2 \tag{17}$$

$$\varepsilon_{in} = {C_\mu}^{3/4} k^{3/2} / C_\mu \delta \tag{18}$$

where δ = boundary layer thickness which may be set to be equal to the flow depth. For stabilizing concerns, constant values for k and ε have been prescribed at the first step of numerical solution process. The bed boundary condition for LES was treated using the log-law-based approximation based on the assumption that the near-wall layer consist of a fully viscous sub-layer and a turbulent layer above it, as follows:

$$u^+ = \begin{cases} z^+ & if \quad z^+ \le 11.6 \\ \kappa^{-1} \ln(9.81 z^+) & if \quad z^+ \ge 11.6 \end{cases} \tag{19}$$

where $\kappa = 0.42$, $u^+ = u/u_*$. The wall-shear stress $\tau_0 = \rho {u_*}^2$ at the bed boundary was calculated using the mentioned wall-function approach without fixing the value of velocity at the bed. Only the normal component of the velocity at the wall is imposed to vanish.

3 RESULTS AND DISCUSSION

In order to validate the developed model, two sets of experimental data have been used. They are rigid bed experiments (Rouland et al. 2005 and Dargahi 1989). For the first experiment the water depth *H = 0.54 m*; pier diameter *D=0.536 m*; the approach velocity u_0 *=0.326 m/s*; Reynolds number of the pier $\mathrm{Re}_D = 1.7 \times 10^5$*; Fr=0.14.* For Dargahi's experiment: $\mathrm{Re}_D = 3.9 \times 10^4$ *H = 0.2 m; D=0.15 m;* u_0 *=0.26 m/s; Fr=0.185;* D_{50}*=0.36 mm.* An O-type mesh with clustering near the solid walls has firstly been generated (Fig. 1). Care was taken to concentrate the mesh towards the cylinder surface to guarantee the good quality of the grid especially in the flow separation region. The computational domain is about 24D in radial direction. A relatively coarse mesh of $80 \times 80 \times 20$ cells is used in this numerical modeling for both RANS and LES models. Although this grid is relatively too coarse for LES models, but it was chosen due to limit performance of the current computers which are commonly used for simulation. It should be noted that in LES modeling the nearest grid to the wall located in the viscous sub-layer i.e. $z^+ < 5$. For the RANS, the value of the Nikuradse roughness of the bed material, k_s was chosen very small (in the order of 10^{-5}) due to smooth walls in the experiments. The calculations were all carried out with a time step of $\Delta t = 0.001$. In order to compare the numerical results of LES, RANS and experimental data we need to use time-averaging process for LES (Cheng et al. 2003). The instantaneous quantities were then averaged over 5000 dimensionless time steps with a temporal resolution of $\Delta t / T_b = \Delta t u_0 / D = 0.016$ (corresponding to an averaging time of 50 large-eddy turnover time T_b). All computations in LES have also been carried out on a personal DELL LATITUDE D830 laptop (Intel Dual Core Processor T7500 @ 2.2 GHz and 2.0 GB RAM). The computational time for a single run in the LES computation, was about 3 weeks on this processor. This computational time could be extremely reduced by using a high performance computer.

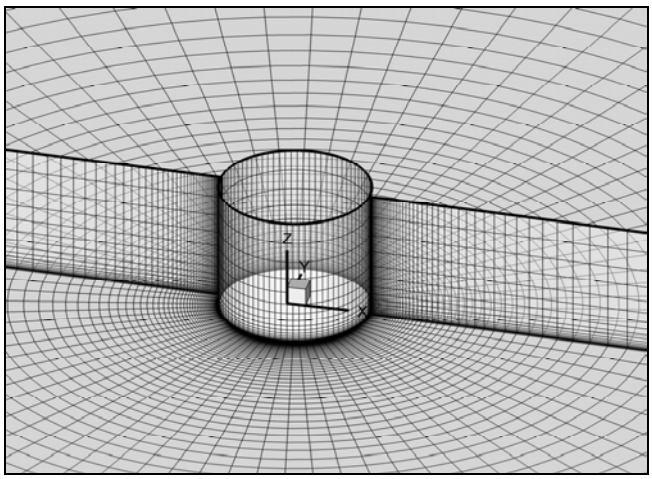

Figure 1. The O-type mesh generated in this simulation with clustering near solid walls.

The time-averaged velocity fields in the vertical plane of symmetry, for different turbulence models and experimental data of Roulund et al. (2005) are depicted in Fig. 2. The predicted flow pattern with the LES and RANS methods around the pier are similar to the flow observed in experiment. Both of the models predicted a clockwise circulation cell and strong down-flow in front of the pier, with the first (and bigger) one being rotated in anticlockwise direction and the second (and smaller) one being rotated in clockwise direction. Also, there is an up-ward flow near the free surface in front of the pier that is in agreement with other experimental observations. This upward flow and consequently the related generated bow wave in shallow flow depths can interfere and counteract the horseshoe vortex and weaken it (Melville 1975). For RANS calculation, no upward flow was appeared in front of the pier near the free surface. However, this upward flow can be seen in the backside of the pier. Also a downward flow near the bed is seen both in the front

and backside of the pier. It should be noted that unfortunately there was no experimental data for the up-half of the depth in Roulund et al.'s experiment. The predicted length of the reattachment flow at the down-stream of the pier for LES was about 1.7 times the pier diameter. The length was about 1.64 for RANS calculations.

Figs. 3 and 4 show the profiles of the mean horizontal velocity (u) and the vertical velocity (w) at the up- and down-stream of the pier for different elevation of the bed in the symmetry line of the domain ($y=0$) obtained from the various numerical simulations together with the experimental data of Roulund et al. (2005). As can be seen from the figures, the numerical of the LES show some discrepancies from experimental data for both horizontal and vertical velocities up-stream of the pier. The discrepancy near the bed for the horizontal velocity at z=5 cm is relatively high and for the vertical velocity with receding from the bed increases; however, at the down-stream of the pier the results are in a relatively good agreement with the experimental data. The discrepancy may partly be due to the bed boundary condition used and/or the estimated Smagorinsky parameter near the wall. In RANS modeling, the results for the vertical velocities are in good agreement with the experiment but the horizontal velocities have relatively high discrepancies with the experimental data. It should be noted that the results of this investigation for both LES and k-ε are in better agreement with the experimental data than the numerical model results of Roulund et al. (2005). They have used the k-ω turbulence model in their calculations. (The results have not been given here for brevity).

Fig. 5 shows the instantaneous horseshoe vortices simulated with LES approach at the upstream of the pier at various time steps. This Variation shows the quasi-periodic behavior of the horseshoe vortex (HV) system near the bed that highly affects the scour process (since HV has the basic role in increasing the bed shear stress near the pier). Using FFT (Fast-Fourier Transform) the frequencies of this vortex shedding can be found from the time variations. Dargahi (1989) indicated rang of 0.1 to 2 Hz for this vortex shedding. This extent range of the frequencies shows that a comprehensive description of the behavior of HVs is not possible. As it can be observed from Fig. 6, there are five horseshoe vortices near the bed at the up-stream of the pier. These time averaged streamlines of LES modeling shows the behavior of the flow at the up-stream of the pier. However, the RANS model could predict only one vortex, as can be seen from Fig. 7. The first vortex (V1) can only be appeared in the LES modeling as can be seen in other experimental data. These vortices (V1 –V5) can also be found in DNS modeling of Yuhi et al. (2000). It seems that the number of these vortices is related to the Re number, the roughness of the bed and boundary layer thickness. The altitude of these vortices decreases from V2 to V5 and they are a little extended to up-stream direction.

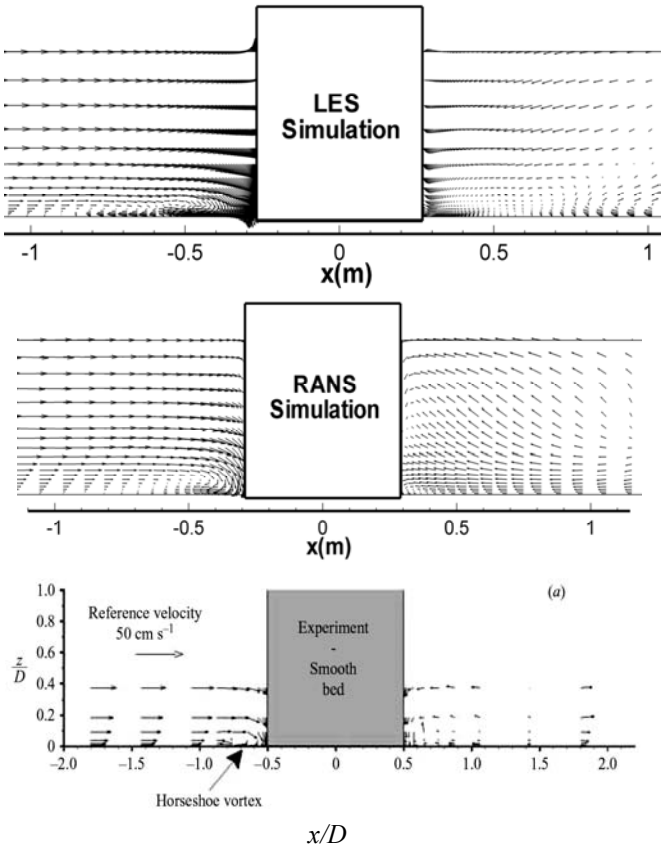

Figure 2. Comparison of the time-averaged velocity vectors of LES, $k-\varepsilon$ and the experiment of Roulund et al. (2005) in the plane of symmetry (y=0).

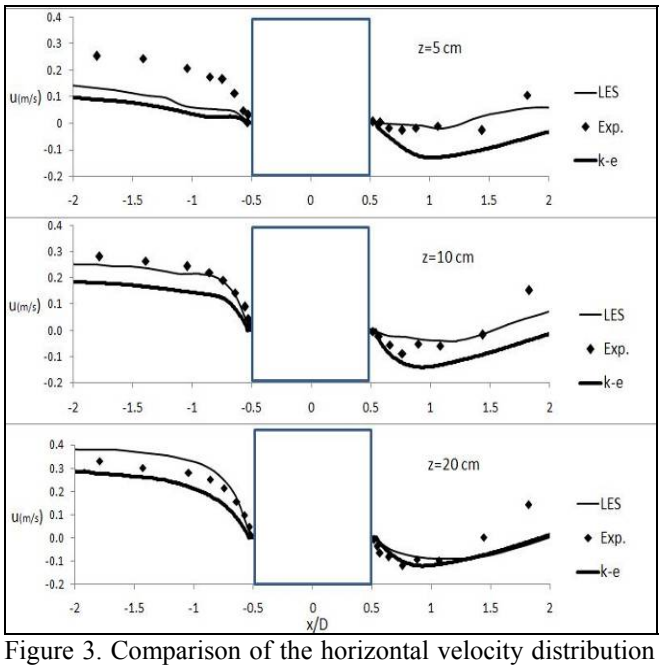

Figure 3. Comparison of the horizontal velocity distribution at up and downstream of the circular pier at z=5cm(top), z=10 cm (mid), z=20 (down) from the bed, between LES, $k-\varepsilon$ and experimental data of Roulund et al. (2005).

No vortex shedding was observed in the RANS computation. LES could capture the vortex shedding of the horseshoe and wake vortices. Also, the time-averaged pressure distribution around the pier for RANS and LES are shown in Fig. 8.

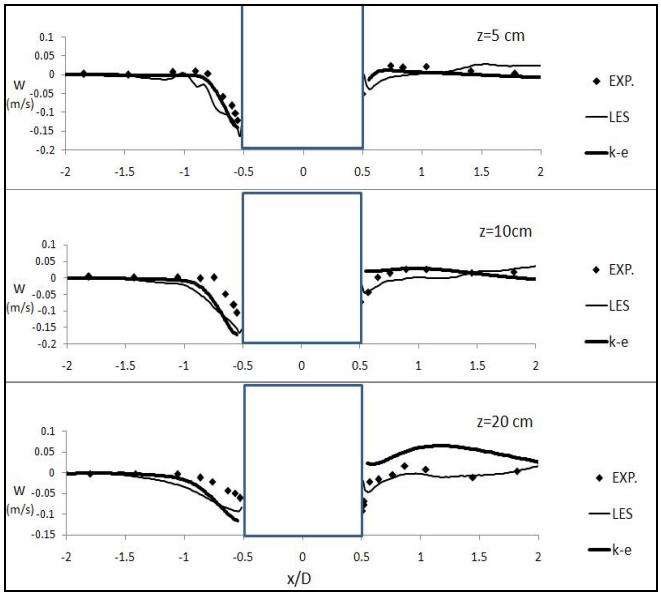

Figure 4. Comparison of the vertical velocity distribution up and downstream of the circular pier for LES, $k-\varepsilon$ and experimental data of Roulund et al. (2005), (z=5cm (top), z=10 cm (mid), z=20 (down) from the bed).

This figure shows the negative values of the pressure field around the pier. In the LES, the minimum value of the pressure occurs in almost 70 degrees from the stagnation point in clockwise direction. In the *k*-ε, the maximum negative value is the same as the LES modeling but its location is in almost 80 degrees from the stagnation point. Also in the *k*-ε, a bulge can be observed in the pressure coefficient distribution in about 100 degrees from the stagnation point, just after the minimum pressure coefficient. In Fig. 9 the contribution of the time-averaged pressure around circular pier for LES and *k*-ε models, are depicted. In the LES model some asymmetries can be observed due to inadequate averaging time of large-eddy turnover time.

Also, as can be seen from Fig. 9, the results of RANS are different from those of the LES. In the RANS the contours of the negative pressure have been stretched to the downstream but in the LES this stretch-ness is accompanied by the encircling space in downstream. Therefore, in this research and for the RANS model, there is not any complete closed vortex circulation for Lee wakes in the free surface layer of the flow and only a reverse flow at the down-stream of the pier can be observed. It should be noted that the other layers have the complete circulation of the Lee wake vortices. Finally, fig. 10 describes the magnitude of the bed shear stress distribution along the symmetry line (y=0) normalized with undisturbed value of the bed shear stress. It is clear from the figure that the magnitude of the bed shear stress is amplified by horseshoe vortices. Therefore, there are about five picks on the graph of bed shear stress for the LES but there is only one pick for the *k*-ε model. The shear stress in LES model is more intensive and extensive than the *k*-ε model. These results indicate that choosing the correct and accurate turbulence model is very important in the scour modeling. It should be noted that the graph is the time-averaged data of LES and the instantaneous flow may have numerous and larger picks than the time-averaged model results.

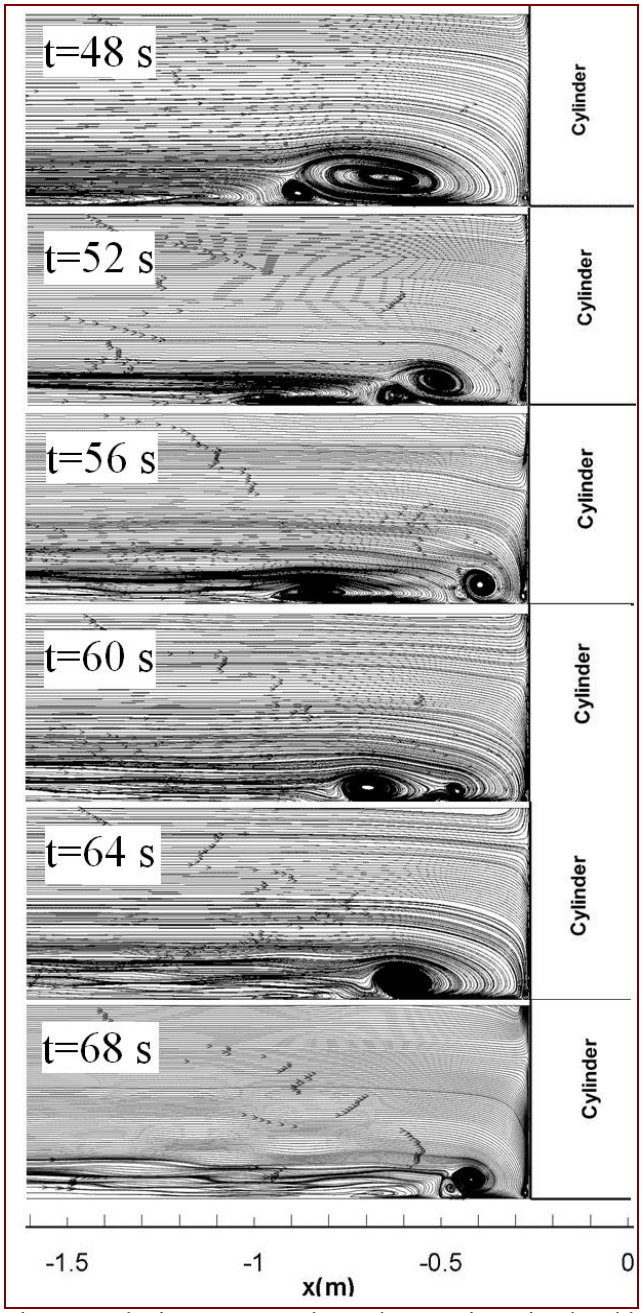

Figure 5. The instantaneous horseshoe vortices simulated by LES approach upstream of the pier at various time steps and in the plane of symmetry (y=0).

4 CONCLUSION

Two different numerical models for simulation of the turbulent flow around the circular pier have been developed. For the first one, RANS calculations with *k*-ε model and for the second one, the LES with constant Smagorinsky parameter have been used. The developed models have been compared with two sets of the laboratory experimental data. As a result, the following conclusions can be drawn:

1) The RANS simulation has relatively sufficient accuracy for engineering application and needs fewer grids for simulation. However, this method has its drawbacks namely, inability to show the correct periodic behavior of the vortex shedding of the both horseshoe and Lee wake vortices and the model results may partly be due to using wall function.
2) The main purpose of numerical modeling of the flow field around the circular pier is to estimate the bed shear stress around the circular pier. The results showed that two turbulent models predicted various bed shear stresses at the up-stream of the cylinder. The bed shear stress in the LES model is more intensive and extensive than the *k*-ε model.
3) In this research study, in contrast to the LES model no vortex shedding has been captured by standard *k*-ε model at both up-stream and down-stream of the pier.
4) The LES model has then shown better results than *k*-ε model, particularly in predicting the horseshoe and Lee wake vortex shedding.
5) Some discrepancies were observed in comparing the model results with the experimental data, there are probably due to: the insufficient resolution near the solid walls, domain extent and number of grid points, using the single time method instead of using the dual time step method and the rigid lid assumption for the free surface that is to some extent questionable.
6) The LES method is very sensitive to the Smagorinsky parameter (C_s). The dynamic procedure for calculating of this parameter may get better results.

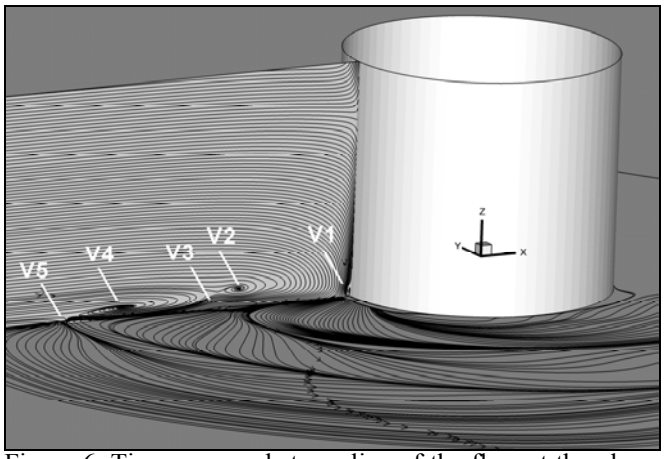

Figure 6. Time averaged streamline of the flow at the plane of symmetry and the near bed plane using LES.

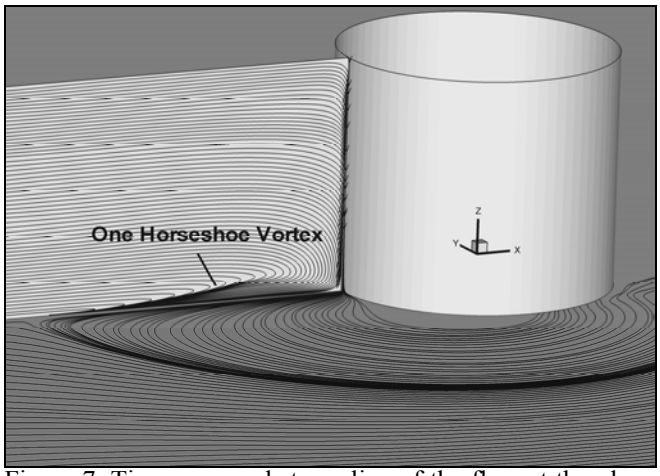

Figure 7. Time averaged streamline of the flow at the plane of symmetry and the near bed plane using RANS.

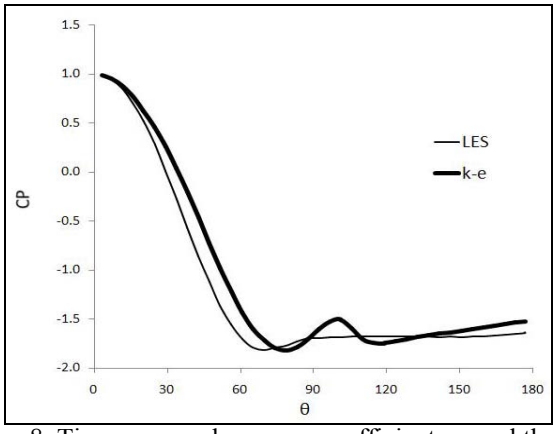

Figure 8. Time-averaged pressure coefficient around the pier for $k-\varepsilon$ and LES modeling.

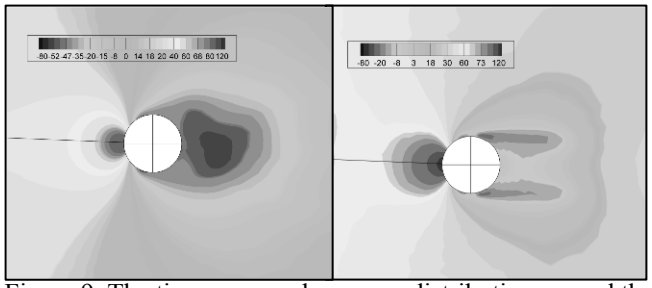

Figure 9. The time-averaged pressure distribution around the pier for LES (left) and $k-\varepsilon$ (right).

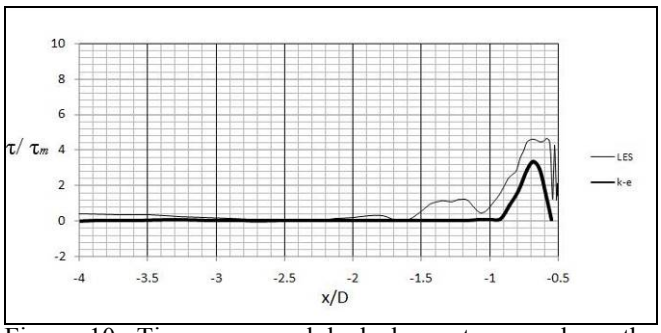

Figure 10. Time- averaged bed shear stresses along the symmetry line (y=0) up stream of the cylinder.

REFERENCES

Breuer, M. 1998. Numerical and modelling influences on large eddy simulations for the flow past a circular cylinder. International Journal of Heat and Fluid Flow, 19, 512–521.

Catalano, P., Wang, M., Iaccarino, G., Moin, P. 2003. Numerical simulation of flow around a circular cylinder at high Reynolds numbers. International journal of heat and fluid flow (24), 463-469.

Cheng, Y., Lien, F. S., Yee, E., Sinclair, R. 2003. A comparison of large Eddy simulations with a standard k–e Reynolds-averaged Navier–Stokes model for the rediction of a fully developed turbulent flowover a matrix of cubes. Journal of Wind Engineering and Industrial Aerodynamics, 91, 1301-1328.

Chorin, A. J. 1967. A numerical method for solving incompressible viscous flow problems. Journal of. Computational Physics, 2, 12-26.

Dargahi, B. 1989. The turbulent flow field around a circular cylinder. Experiments in Fluids; 8: 1–12.

Dargahi, B. 1990. Controlling mechanism of local scouring. Journal of Hydraulic Engineering, ASCE; 116(10); 1197–1214.

Gresho, PM. 1991. Some current CFD issues relevant to the incompressible Navier–Stokes equations. Computer Methods in Applied Mechanics and Engineering, 87:201–252.

Gushchin, V. A., Kostomarov, A. V., Matyushin, P. V., Pavlyukova, E. R. 2002. Direct numerical simulation of the transitional separated fluid flows around a sphere and a circular cylinder. Journal of Wind Engineering and Industrial Aerodynamics 90, 341–358

Hakimzadeh, H., Falconer, R., A. 2007. Layer integrated modeling of three-Dimensional recirculating flows in model tidal basins. Journal of waterway, Port, Coastal, and ocean engineering, ASCE, vol. 133-5, 324-332.

Kim, W-W., Menon, S. 1999. An unsteady incompressible Navier–Stokes solver for large eddy simulation of turbulent flows. International Journal for Numerical Methods in Fluids, 31:983–1017.

Leonard, B. P. 1975. A stable and accurate convective modelling procedure based on quadratic upstream interpolation. Computing Methods in Applied Mechanical Engineering 1979, 19: 59–98.

Li, C. W., Yu, T. S. 1996. Numerical investigation of turbulent shallow recirculating flows by a quasi-three dimensional $k-\varepsilon$ model. International Journal for Numerical Methods in Fluids, 23, 485-501.

Luda, P., Kozel, K., Prihoda, J. 2008. Numerical solution of 2D and 3D viscous incompressible steady and unsteady flows using artificial compressibility method. International journal for numerical methods in fluids. 56: 1399-1400.

Majumdar, S., Rodi, W. 1989. Three-dimensional computation of flow past cylindrical structures and model cooling towers. Build. Environ. 24 (1), 3–22.

Melville, B. W. 1975. Local scour at bridge site. Rep. No. 117, school of Engineering, the university of Auckland, New Zeland.

Nagata, N., Hosoda, T., Nakato, T., Muramoto, Y. 2005. Three-dimensional numerical model for flow and bed deformation around river hydraulic structures. Journal of Hydraulic engineering, ASCE, 131, 1074-1087

Olsen, N. R. B., Melaaen, M. C. 1993. Three-dimensional calculation of scour around cylinders. Journal of. Hydraulic Engineering, ASCE 119, 1048–1054.

Rodi, W. 1997. Comparison of LES and RANS calculation of the flow around bluff bodies. Journal of Wind Engineering and Industrial Aerodynamics, 69–71, 55–75.

Roulund, A., Sumer, B. M., Fredsoe, J., Michelsen, J. 2005. Numerical and experimental investigation of flow and scour around a circular pile . J. Fluid Mech. vol. 534, pp. 351–401.

Rhie, C. M., Chow, WL.1983. Numerical study of the turbulent flow past an airfoil with trailing edge separation. AIAAJournal, 21(11), 1525–1532.

Smagorinsky, J., 1963. General circulation experiments with the primitive equations. I. The basic experiment. Monthly Weather Review 91 (3), 99–164.

Salaheldin, T. M., Imran, J., Chaudhry, H. 2004. Numerical modeling of three-dimensionalflow field around circular pier. Journal of hydraulic engineering, ASCE 130(2),91-100.

Tseng, M. H., Yen, C. L., Song, C. C. S. 2000. Computation of three-dimensional flow around square and circular piers. International Journal of Numerical Methods in Fluids 34, 207–227.

Wissink, J. G., Rodi, W. 2008. Numerical study of the near wake of a circular cylinder. International Journal of Heat and Fluid Flow. 29(4), 1060-1070.

Yuhi, M., Ishida, H., Umeda, S. 2000. Anumerical study of three-dimensional flow fields around a vertical cylinder mounted on a bed. Coastal structures 99, Balkema, Roterdam, 783-792.